Supporting Information

Shapeable Aerogels of Metal-Organic-Frameworks Supported by Aramid Nanofibrils for Efficient Adsorption and Interception

Lu Zong[†, 1], *Yongqiang Yang*[†, 2], *Hui Yang*[1], *Xiaochen Wu*[1,3,*]

[1]Department of Pharmacy, College of Chemical Engineering, Qingdao University of Science and Technology, Qingdao 266042, China

[2]National Graphene Products Quality Supervision and Inspection Center (Jiangsu), Jiangsu Province Special Equipment Safety Supervision Inspection Institute·Branch of Wuxi, Yanxin Road 330, Wuxi 214174, PR China

[3]Key Laboratory of Pharmaceutical Research for Metabolic Diseases, Qingdao University of Science and Technology, Qingdao 266042, China

Corresponding Author: (X. Wu) wxcguest@126.com

†L. Zong and Y. Yang contributed equally to this work.

Additional Experimental

ZIF-67, HKUST-1 and Ni-HITP hybrid aerogels were obtained in a similar way as ZIF-8 hybrid aerogels. For example, ZIF-67 hybrid aerogels were acquired with 4.9 mg/mL of cobalt nitrate and 5.5 mg/mL of 2-methylimidazole at 80 °C for 12 h in methanol, HKUST-1 decorated aerogels were acquired with 4.1 mg/mL of copper nitrate and 4.1 mg/mL of trimesic acid at 25 °C for 12 h in ethanol, while Ni-HITP hybrid aerogels were acquired with 2.2 mg/mL of nickel nitrate, 3.3 mg/mL of HITP and 1.3 M of $NH_3 \cdot H_2O$ in H_2O at 70 °C for 12 h (ref: ACS Nano 2019, 13 (8), 9578-9586).

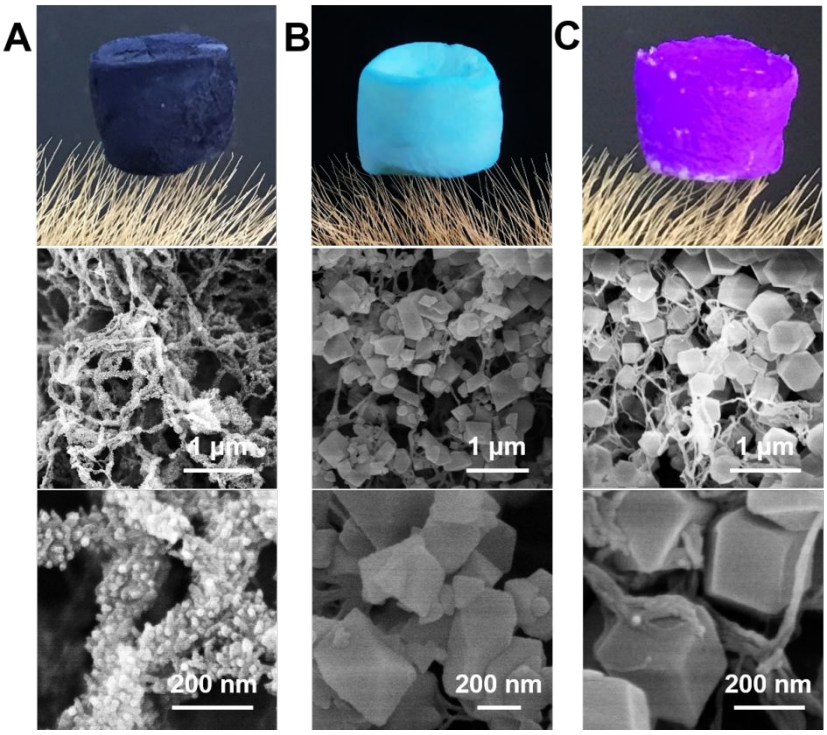

Figure S1. Photographs and SEM images of the MOFs hybrid aerogels. (A) Ni-HITP, (B) HKUST-1, and (C) ZIF-67 hybrid aerogels.

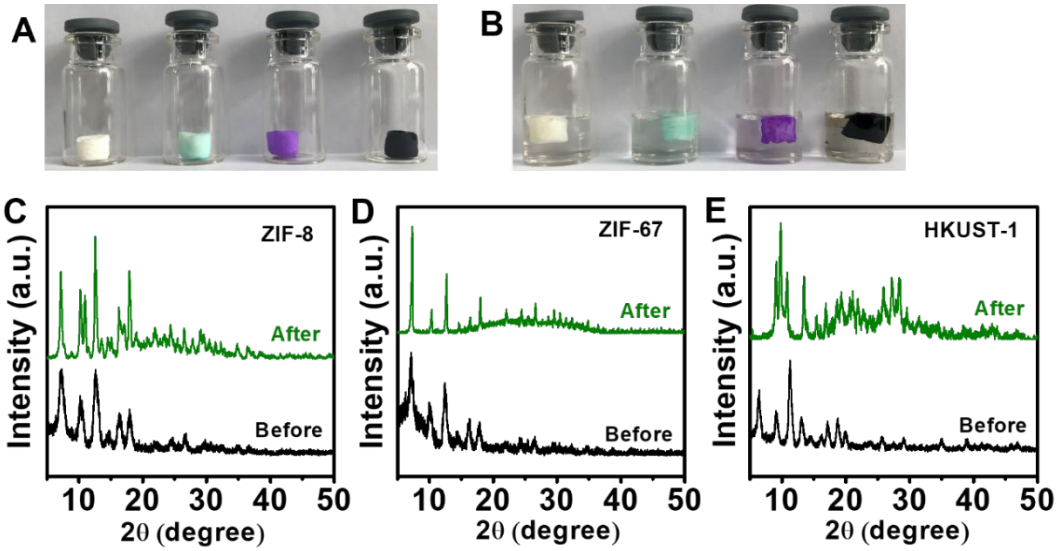

Figure S2. (A-B) Photographs of MOFs hybrid aerogels under (A) dry condition and immersing in H_2O for 24 h. From left to right: ZIF-8, HKUST-1, ZIF-67 and Ni-HITP hybrid aerogels. (C-E) XRD patterns of MOFs hybrid aerogels before and after immersing in H_2O for 24 h.

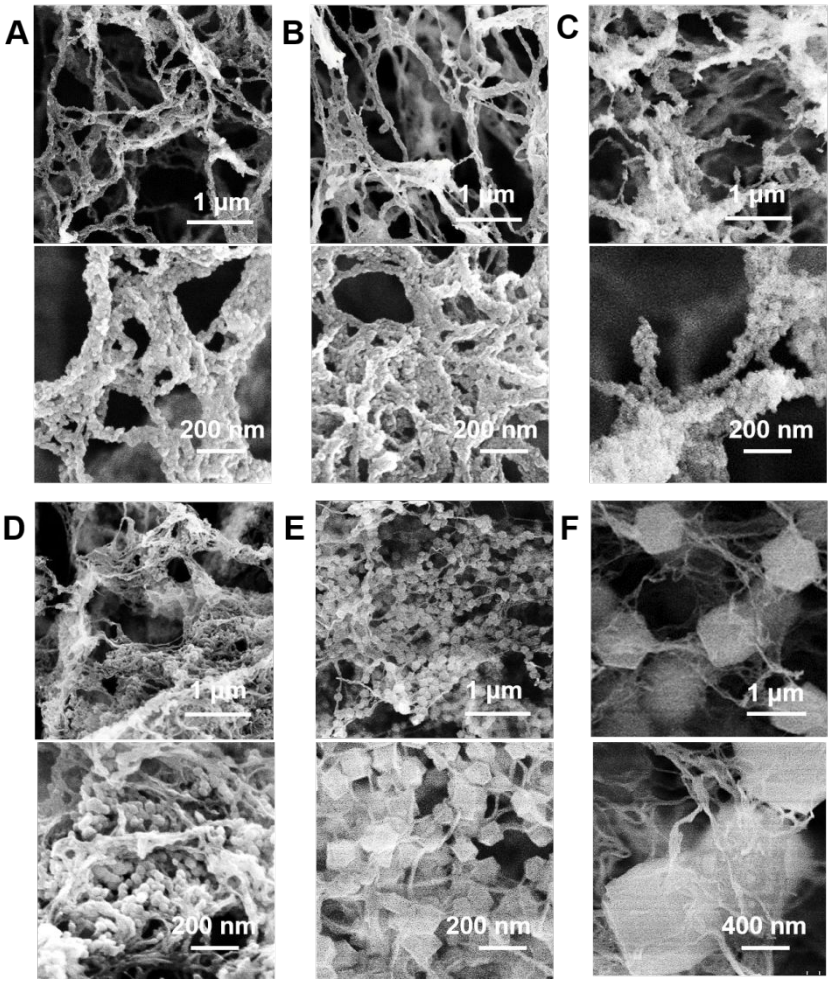

Figure S3. SEM images of ZIF-8 hybrid aerogels with different ZIF-8 contents: (A) 19 wt.%, (B) 36 wt.%, (C) 54 wt.%, (D) 61 wt.%, (E) 77 wt.%, and (F) 84 wt.%.

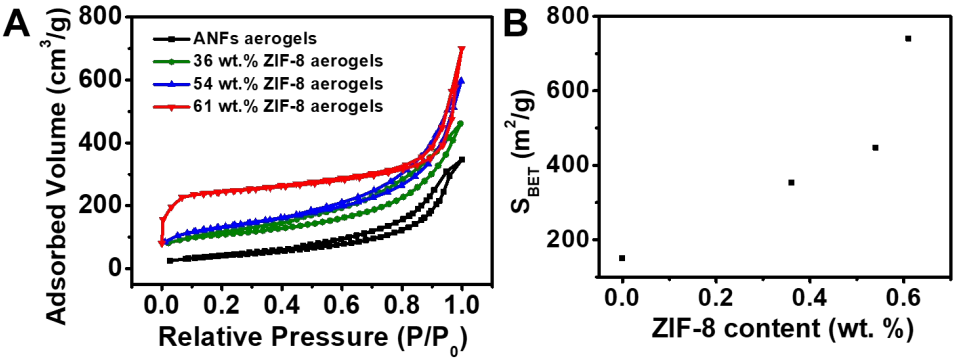

Figure S4. (A) Nitrogen adsorption−desorption analysis and (B) specific surface area of ZIF-8 hybrid aerogels.

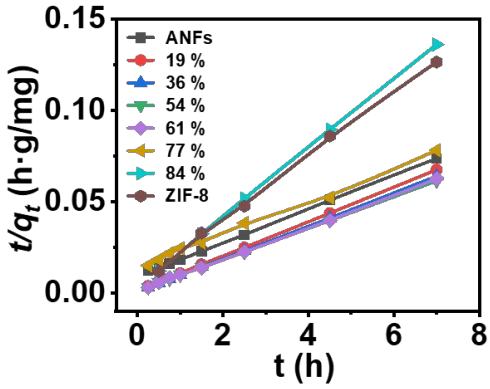

Figure S5. Pseudo second-order plots fitted with the data from Figure 3B (based on the mass of aerogels). $t/q_t=1/(kq_e^2)+t/q_e$, where t referred to the contact time (h), k referred to the second-order rate constant (g/(mg·h)), q_e referred to the equilibrium uptake amount of dyes (mg/g), q_t referred to the adsorption capacity at different times.

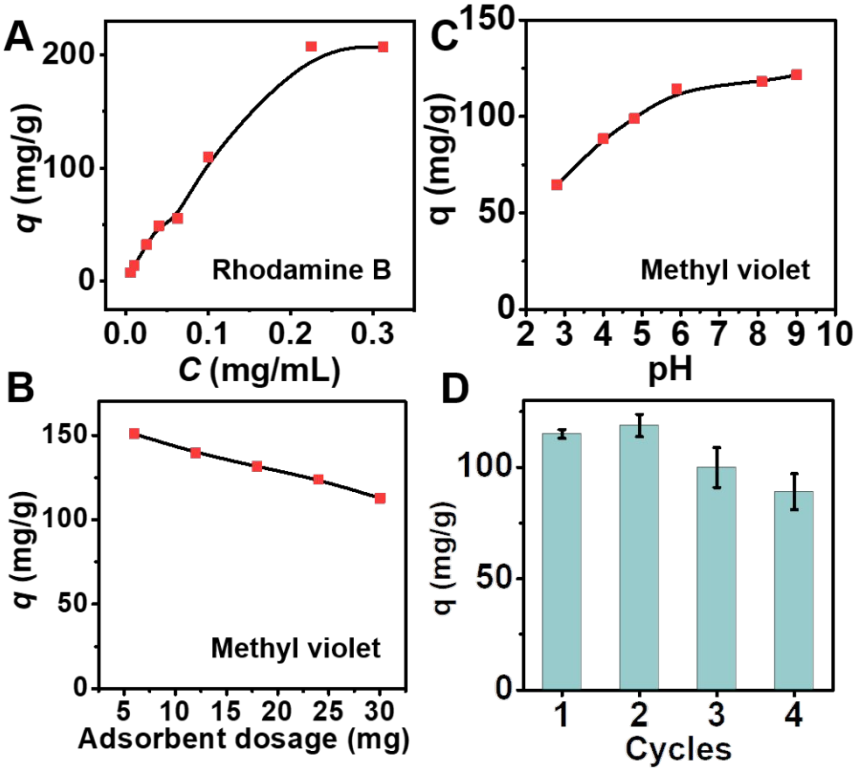

Figure S6. (A) Adsorption of rhodamine B *versus* its initial concentration, using ZIF-8 hybrid aerogels with 54 wt.% ZIF-8 content. (B-C) Effect of (B) the amount of ZIF-8 aerogels and (C) pH on the adsorption of methyl violet. (D) The reusability of ZIF-8 aerogels.

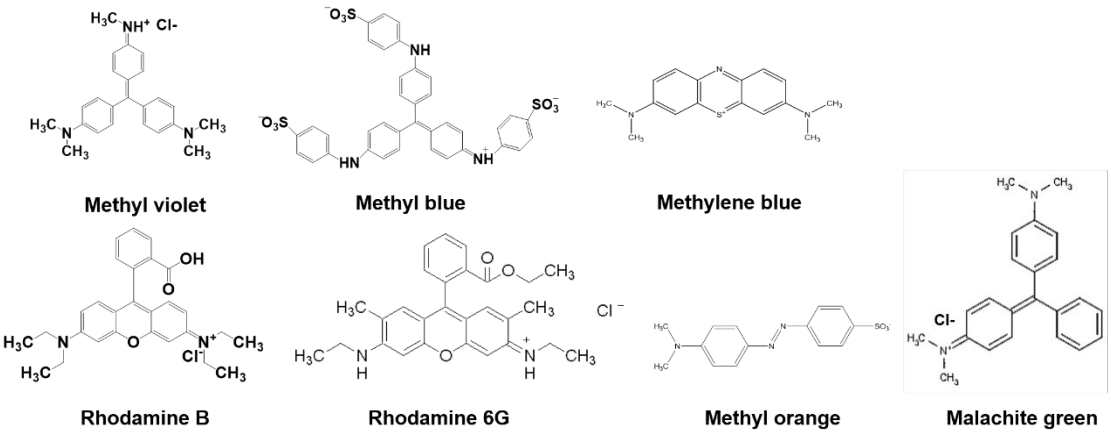

Figure S7. Molecular structures of dyes used.

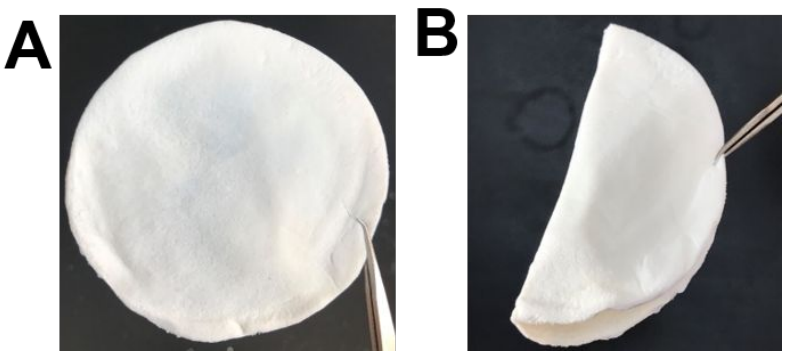

Figure S8. Photographs of (A) ZIF-8 (54 wt.%) hybrid aerogel and (B) folded aerogel showing flexibility.

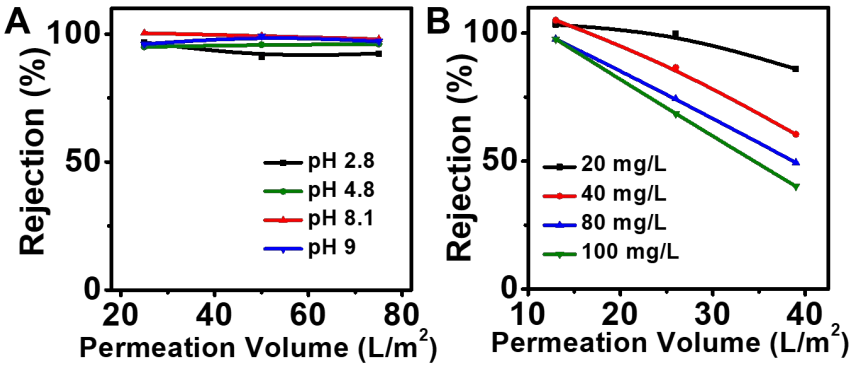

Figure S9. Effect of (A) pH and (B) the concentration of methyl violet on its rejection, under a pressure of 0.5 bar and aerogel thickness of ~0.87 mm. The concentration of methyl violet was 10 mg/L in (A).

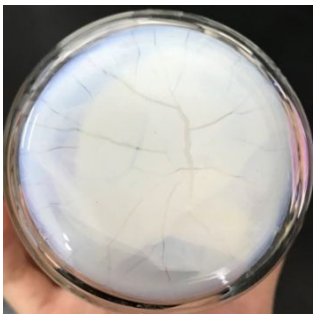

Figure S10. Photograph of ANFs aerogel with thickness of ~0.87 mm. It was fragile with lots cracks after the freeze-drying.

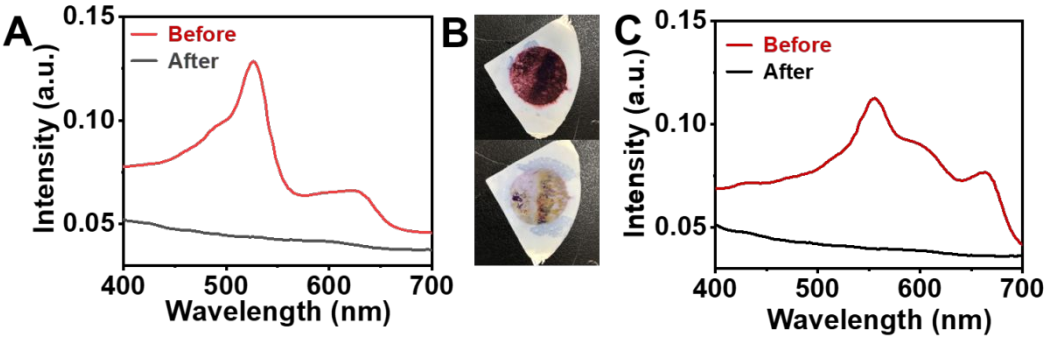

Figure S11. (A, C) Uv-vis spectra of mixed dyes before and after passing through the ZIF-8 (54 wt.%) hybrid aerogels. (B) Photographs of the upper and nether sides of ZIF-8 hybrid aerogels after filtration. Mixed dyes: (A) 1 mg/L methyl blue + 1 mg/L rhodamine 6G + 1 mg/L methyl orange; (C) 1 mg/L methylene blue + 1 mg/L methyl violet + 1 mg/L rhodamine B + 1 mg/L methyl orange + 1 mg/L malachite green.

Table S1. Detailed synthesis conditions for ZIF-8 hybrid aerogels (Reactions were conducted in methanol at 25 °C).

Sample ID	$C_{ANFs\ gels}$ (mg/mL)	C_{Zn2+} (mg/mL)	C_{ligand} (mg/mL)
19 wt. % ZIF-8 aerogels	0.8	0.2	0.44
36 wt. % ZIF-8 aerogels	0.8	0.5	1.1
54 wt. % ZIF-8 aerogels	0.8	5	11
61 wt. % ZIF-8 aerogels	0.8	10	22
77 wt. % ZIF-8 aerogels	0.8	30	65.7
84 wt. % ZIF-8 aerogels	0.8	50	110

Table S2. Adsorption capacity of ZIF-8 hybrid aerogels for methyl violet compared with other reported MOFs-based systems.

Adsorbent	Dye concentration (mg/L)	Kinetics	Second-order rate constant ($g\cdot mg^{-1}\cdot h^{-1}$)	Experimental adsorption capacity (mg/g)	References
ZIF-8 hybrid aerogels	100	pseudo-second-order	0.55	113.7	This work
ZIF-8 templated with nanocellulose aerogels	10	pseudo-second-order		~27	[1]
Multi-walled carbon nanotubes/$Mn_{0.8}Zn_{0.2}Fe_2O_4$ nanoparticles	5	pseudo-second-order	0.028	5	[2]
Reduced graphene oxide/ZIF-67 aerogel	500	pseudo-second-order		1714.2	[3]
Reduced graphene oxide/ZIF-67 aerogel	100	pseudo-second-order		~200	[3]
Activated carbon-HKUST-1-MOF hybrid	10	pseudo-second-order	0.69	18.25	[4]
Copper coordination polymer with dithiooxamide (H_2dtoaCu)	100	pseudo-second-order	0.222	68.01	[5]
Anionic zeolite-like metal–organic framework $[(CH_3)_2NH_2]_6[Sr_{13}(O)$	1000			184	[6]

$_3$(BTTC)$_8$(OH)$_2$(H$_2$O)$_{16}$]·xS					
UPC-102-Zr	4 ×10^{-5} mol/L			182	[7]

Table S3. Flux and rejection of ZIF-8 hybrid aerogels during the filtration of dyes compared with other reported MOFs-based systems.

Samples	Dyes	Dye concentration	Flux (L· m^{-2}·h^{-1}·bar^{-1})	Rejection	References
ZIF-8 hybrid aerogels	methyl violet	10 mg/L	650	> 97 %	This work
Cellulose nanofibrous membrane with ZIF-8	janus green B	10 mg/L	85.8 L·m^{-2}h^{-1}	>97 %	[8]
Partial reduction graphene oxide membrane	methylene blue	0.01-0.05 mM	98.5	99.3 %	[9]
UiO-66-(COOH)$_2$/ partial reduction graphene oxide membrane	rhodamine B	0.01-0.05 mM	93.0-95.0		[9]
UiO-66 on alumina membrane	humic acid	1000 mg/L	34	99 %	[10]
Hydrophilic regenerated cellulose support membrane with UiO-66 nanoparticles	methylene blue	1.0 μmol	785.8	100 %	[11]
MOF/GO membrane	methyl orange, direct red 80	200 mg/L	~16 kg·m^{-2}h^{-1}	~97 %	[12]
NH2-UiO-66 PE MMM-86%	orange G	100 mg/L	115.9	99 %	[13]
NH2-UiO-66 PE MMM-86%	fuchsine acid	100 mg/L	111.4	99.1%	[13]

References:

(1) Zhu, L.; Zong, L.; Wu, X.; Li, M.; Wang, H.; You, J.; Li, C. Shapeable Fibrous Aerogels of Metal–Organic-Frameworks Templated with Nanocellulose for Rapid and Large-Capacity Adsorption. *ACS Nano* **2018,** *12* (5), 4462-4468, DOI: 10.1021/acsnano.8b00566.

(2) Gabal, M. A.; Al-Harthy, E. A.; Al Angari, Y. M.; Salam, M. A. MWCNTs Decorated with $Mn_{0.8}Zn_{0.2}Fe_2O_4$ Nanoparticles for Removal of Crystal-Violet Dye from Aqueous Solutions. *Chem Eng J* **2014,** *255*, 156-164, DOI: 10.1016/j.cej.2014.06.019.

(3) Yang, Q. X.; Lu, R.; Ren, S. S.; Chen, C. T.; Chen, Z. J.; Yang, X. Y. Three Dimensional Reduced Graphene Oxide/ZIF-67 Aerogel: Effective Removal Cationic and Anionic Dyes from Water. *Chem Eng J* **2018,** *348*, 202-211, DOI: 10.1016/j.cej.2018.04.176.

(4) Azad, F. N.; Ghaedi, M.; Dashtian, K.; Hajati, S.; Pezeshkpour, V. Ultrasonically Assisted Hydrothermal Synthesis of Activated Carbon-HKUST-1-MOF Hybrid for Efficient Simultaneous

Ultrasound-Assisted Removal of Ternary Organic Dyes and Antibacterial Investigation: Taguchi Optimization. *Ultrason Sonochem* **2016,** *31*, 383-393, DOI: 10.1016/j.ultsonch.2016.01.024.
(5) Li, X.; Zheng, L.; Huang, L.; Zheng, O.; Lin, Z.; Guo, L.; Qiu, B.; Chen, G. Adsorption Removal of Crystal Violet from Aqueous Solution Using a Metal-Organic Frameworks Material, Copper Coordination Polymer with Dithiooxamide. *J Appl Polym Sci* **2013,** *129* (5), 2857-2864, DOI: 10.1002/app.39009.
(6) Shen, Y.; Fan, C.-C.; Wei, Y.-Z.; Du, J.; Zhu, H.-B.; Zhao, Y. An Anionic Zeolite-Like Metal-Organic Framework (AZMOF) with Moravia Network for Organic Dyes Absorption through Cation-Exchange. *Dalton Trans* **2016***, 45,* 10909-10915, 10.1039.C6DT01697A.
(7) Fan, W.; Wang, X.; Xu, B.; Wang, Y.; Liu, D.; Zhang, M.; Shang, Y.; Dai, F.; Zhang, L.; Sun, D. Amino-Functionalized MOFs with High Physicochemical Stability for Efficient Gas Storage/Separation, Dye Adsorption and Catalytic Performance. *J Mater Chem A* **2018,** *6* (47), 24486-24495, DOI: 10.1039/c8ta07839d.
(8) Song, Y.; Seo, J. Y.; Kim, H.; Beak, K.-Y. Structural control of Cellulose Nanofibrous Composite Membrane with Metal Organic Framework (ZIF-8) for Highly Selective Removal of Cationic Dye. *Carbohyd. Polym.* **2019,** *222*, 115018-115018, DOI: https://doi.org/10.1016/j.carbpol.2019.115018.
(9) Zhang, P.; Gong, J.-L.; Zeng, G.-M.; Song, B.; Liu, H.-Y.; Huan, S.-Y.; Li, J. Ultrathin Reduced Graphene Oxide/MOF Nanofiltration Membrane with Improved Purification Performance at Low Pressure. *Chemosphere* **2018,** *204*, 378-389, DOI: https://doi.org/10.1016/j.chemosphere.2018.04.064.
(10) Abdullah, N.; Rahman, M. A.; Dzarfan Othman, M. H.; Jaafar, J.; Aziz, A. A. Preparation, Characterizations and Performance Evaluations of Alumina Hollow Fiber Membrane Incorporated with UiO-66 Particles for Humic Acid Removal. *J. Membrane Sci.* **2018,** *563*, 162-174, DOI: https://doi.org/10.1016/j.memsci.2018.05.059.
(11) Trinh, D. X.; Tran, T. P. N.; Taniike, T. Fabrication of New Composite Membrane Filled with UiO-66 Nanoparticles and Its Application to Nanofiltration. *Sep. Purif. Technol.* **2017,** *177*, 249-256, DOI: https://doi.org/10.1016/j.seppur.2017.01.004.
(12) Ma, J.; Guo, X.; Ying, Y.; Liu, D.; Zhong, C. Composite Ultrafiltration Membrane Tailored by MOF@GO with Highly Improved Water Purification Performance. *Chem. Eng. J.* **2017,** *313*, 890-898, DOI: https://doi.org/10.1016/j.cej.2016.10.127.
(13) Wang, H.; Zhao, S.; Liu, Y.; Yao, R.; Wang, X.; Cao, Y.; Ma, D.; Zou, M.; Cao, A.; Feng, X.; Wang, B. Membrane Adsorbers with Ultrahigh Metal-Organic Framework Loading for High Flux Separations. *Nat. Commun.* **2019,** *10* (1), 4204-4204, DOI: 10.1038/s41467-019-12114-8.